Astron. Astrophys. 317, 232–243 (1997)

ASTRONOMY
AND
ASTROPHYSICS

Evidence for highly inhomogeneous mm-wave sources during the impulsive flare of May 9, 1991

R. Herrmann[1], **A. Magun**[1], **P. Kaufmann**[2], **E. Correia**[3], **J.E.R. Costa**[3], **M.E. Machado**[4], **and G.J. Fishman**[5]

[1] Institute of Applied Physics, University of Bern, Bern, Switzerland
[2] Dept. of Physics, University of Alabama in Huntsville Alabama, USA and CONAE, Buenos Aires, Argentina
[3] CRAAE/NUCATE, UNICAMP, Campinas, SP, Brazil
[4] CRAAE/INPE, S. Paulo, SP, Brazil
[5] Space Science Laboratory, NASA/MSFC, Alabama, USA

Received 16 February 1994 / Accepted 4 May 1996

Abstract. In this paper multiwavelength observations of an impulsive flare of May 9, 1991 are presented. This event was observed with the 48 GHz multibeam focal array used at the Itapetinga radio telescope, the microwave patrol telescopes at Bern and the BATSE high time resolution hard X-ray spectrometer on board CGRO. While spatially unresolved low sensitivity observations show two major impulsive peaks, the mm-wave observations with the ability of spatially high resolved tracking of the emission centroids suggest a primarily bipolar source configuration. For the first time two mm-wave sources with a spacing below the HPBW could be separated with the multibeam technique. The general features of the observations are explained as emission of partially trapped electrons. Furthermore we present evidence for highly inhomogeneous substructures within one of the two mm-wave sources for which the positional scatter of the emission center, within 2 s, is less than 2".

Key words: Sun: flares – Sun: radio radiation – Sun: X-rays

1. Introduction

Solar microwave bursts are generally assumed to be due to energetic electrons of several hundred keV to some MeV, which gyrate around magnetic field lines and hence emit electromagnetic radiation in the microwave range. On the other hand, hard X-ray emission is bremsstrahlung emitted by energetic electrons of some ten to some hundred keV. Attempts to get a consistent interpretation of the hard X-ray observations resulted in the development of the thick and thin target models. While the thick target model requires a high density plasma and hence only explains emission from sources low in the corona, the thin target model predicts emission from the coronal part of a loop. However the thick target model does not explain the emission from behind the limb events, and the efficiency of the thin target model is too low to be consistent with the observed microwave flux in most cases. This resulted in the development of the 'trap plus precipitation' model (Hudson 1972; Melrose et Brown 1976). This model combines the thick and the thin target ideas: while thin target hard X-ray and the microwave emission result from electrons trapped in magnetic loops, electrons with low pitch angles precipitate into dense chromospheric regions where they efficiently emit X-rays by bremsstrahlung (e.g. Vilmer 1987, for a review). Already the first analytical paper (Melrose et Brown 1976) predicted energy dependent delays of the more energetic hard X-ray emission, due to the energy dependence of coulomb scattering into the loss cone. More accurate analytical and numerical calculations (MacKinnon et al. 1983; Trottet et Vilmer 1984), as well as studies including wave particle interactions (Bespalov et al. 1987) confirmed this picture, but also added new insights like the behaviour in case of moderate and strong diffusion.

In this paper we present observations of the event of May 9, 1991 in the microwave range with high time as well as high spatial resolution, together with high time resolution hard X-ray observations. The combined analysis of timing and spectral features of the emission in the microwave and hard X-ray band, together with the microwave polarization properties and the spatially resolved 48 GHz observations, let us suggest that the emission of this impulsive event is governed by the 'trap plus precipitation' mechanism.

Finally we present, for the first time, evidence for fast and most probably small structures at 48 GHz that indicate the presence of multiple highly inhomogeneous microwave sources. Most of the spatially resolved microwave observations that are available today show geometrical complexity (e.g. Alissandrakis 1986, for a review) and the presence of several spatially separated sources at mm wavelengths has already been suggested for two different events (Herrmann et al. 1994, Costa 1994, private communication). Furthermore, spatially resolved

Send offprint requests to: A. Magun

hard X-ray observations made by the Japanese YOHKOH satellite revealed numerous complex structures (e.g. Sakao et al. 1992). However there exist only a few observations so far that presented evidence for small scale inhomogeneities at mm wavelengths (Kundu et al. 1991; White and Kundu 1992).

The next section contains a short description of the instruments that provided the observations while in the following section microwave and hard X-ray total flux observations are presented. The fourth section presents the spatially resolved mm wave observations while the interpretation of the observations is presented in the last part of the paper.

2. Instrumentation

Three observatories have been involved in the observations: the Itapetinga Radio Observatory near São Paulo using a multibeam front-end array at the focus of the 13.7 m mm-antenna, the Bern Radio Observatory with its patrol instruments observing the full Sun at discrete microwave frequencies and the BATSE hard X-ray spectrometer on board the Compton Gamma Ray Observatory satellite (CGRO).

2.1. Total flux observations

At the Bern Observatory full disk patrol observations of the Sun at 3.1, 5.2, 8.4, 11.8, 19.6, 35.0 and 50.0 GHz are carried out with a time resolution of 0.1 s at RCP and LCP (e.g. Bruggmann et Magun 1990). The sensitivity limit is $\cong$ 10 sfu depending on the frequency. Short sky observations performed every 3 hours allow flux calibration using SGD quiet sun fluxes.

In this paper we use high time resolution, spectrally-resolved observations recorded by the Burst and Transient Source Experiment (BATSE, Fishman et al. 1989) aboard the Compton Gamma Ray Observatory (CGRO). BATSE has higher sensitivity and larger area than previous instruments and can hence provide the required statistically significant spectra on short timescales. The instrument consists of eight wide-field large-area detector modules (LADs) mounted at the eight corners of the spacecraft, which continously monitor the sky and provide continous solar viewing outside the spacecraft eclipses. When significant increases are detected in the discriminator rates at energies above 60 keV on any of the three timescales (64, 256 or 1024 ms), a burst trigger signal starts its high time resolution burst mode in which the 4 energy channel, 64 ms data used in this study are recorded.

2.2. Observations with a multibeam focal array

The millimeter wave reflector of the Itapetinga Radio Observatory is used with an array of 5 total intensity receivers at its focus producing 5 beams at 48 GHz. The high sampling frequency of 1 kHz for all channels and the multibeam technique allow the fast tracking of mm-wave emission centers with a relative position accuracy of 5 ” to 20 ” (Georges et al. 1989; Herrmann et al. 1992). Furthermore its sensitivity limit of less than 0.1 s.f.u. makes the instrument suitable for the observation of weak events. Absolute flux calibration is possible within about $\pm$20%. Data processing and the algorithm for position calculation of one integrated emission center have already been described in detail (Herrmann et al. 1992) and are therefore only briefly summarized. After gain and offset corrections the flux of the quiescent Sun is subtracted to separate the burst emission. An algorithm compares ratios of measured fluxes in different beams with those calculated for all possible source positions within the field of view. The most probable position is hence defined by the smallest deviation between the calculated and the measured flux ratios. This method does in general not allow to separate multiple sources that emit at the same time if their angular distance is smaller than the HPBW. Nevertheless the following sections will show that in case of a special source geometry, relative to the focal array, a separation may be possible.

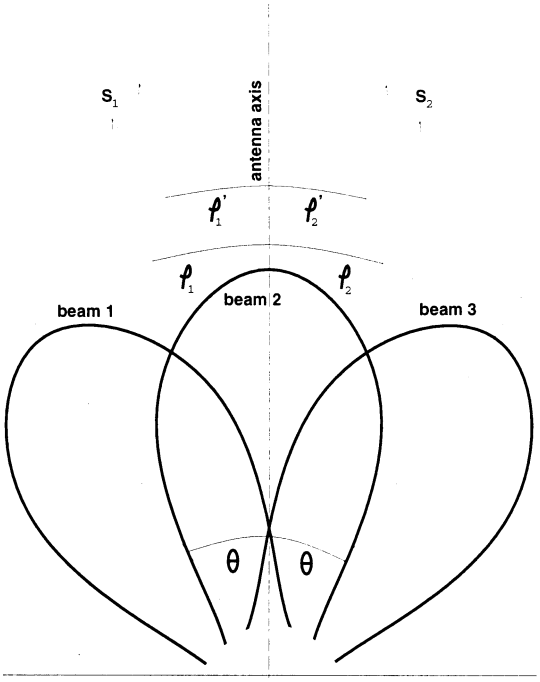

Fig. 1. Sketch of a simple antenna beam pattern of three intersecting beams observing two sources that emit at the same time.

For simplicity the one dimensional geometry illustrated in Fig. 1 is discussed first. The simple beam pattern consists of three beams. Beams 1 and 3 are inclined with respect to the antenna axis by -θ and +θ respectively while beam 2 is aligned. This beam pattern is used to observe two small sources (S_2 and S_1) at an angular distance of $\pm\varphi$ from the antenna axis. Source 1 is assumed to be brighter than source 2. In a first step, beams 1 and 2 are used to calculate the position of the emission center relative to the antenna axis as described above. The resulting position $\varphi_1^{'}$ will be close to the position of S_1 but shifted towards beam 2. The response of beam 1 to emission of S_2 is strongly suppressed due to its low beam gain in the direction of S_2. Switching off beam 1 and using beam 2 and 3 instead, the emission center at a different position $\varphi_2^{'}$ is obtained in a

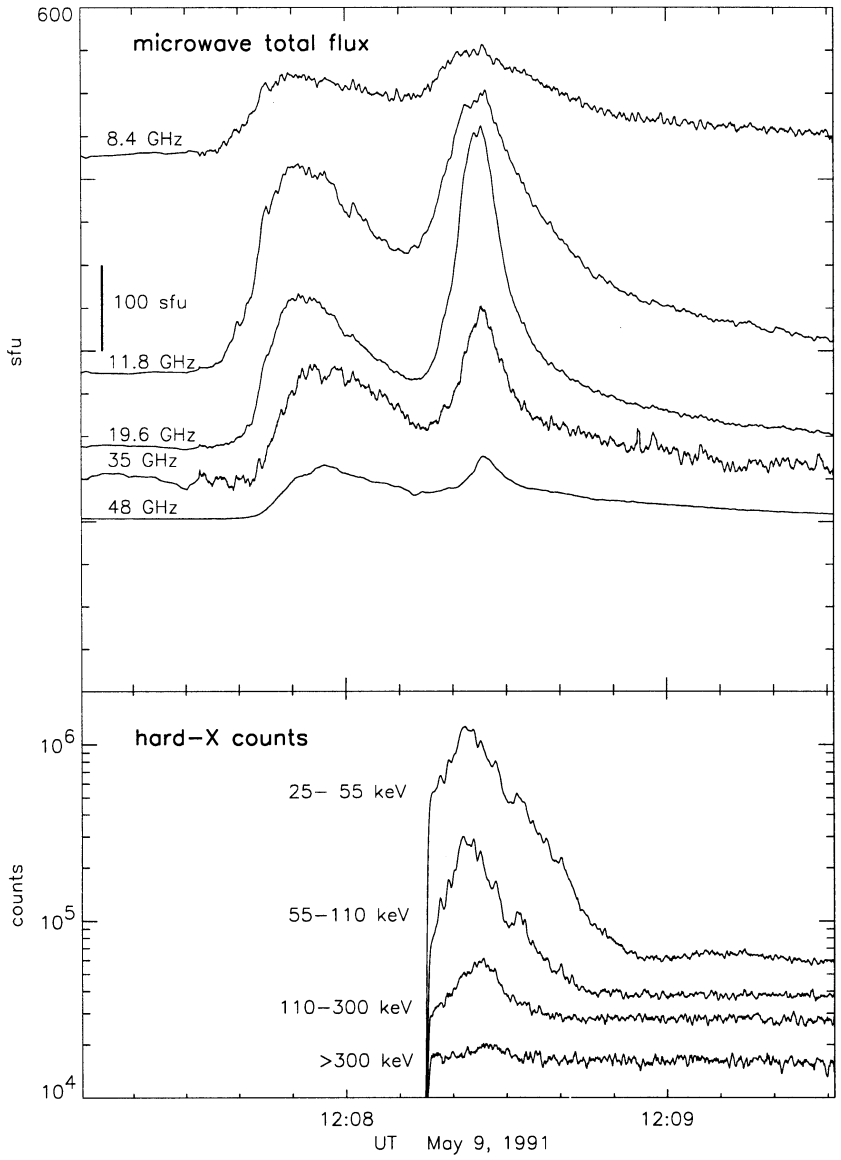

Fig. 2. Microwave total flux observations of the impulsive flare of May 9, 1991. Flux time profiles at 8.4, 11.8, 19.6 and 35 GHz have been recorded at the Bern Observatory while the 48 GHz total power profile results from a summation over all 48 GHz channels of the Itapetinga Observatory. The photon count time profiles which have been obtained with the 4 high time resolution channels of the BATSE hard X-ray spectrometer on board GRO are plotted below. Observations are only available after 12:08:15 UT due to the satellite passing through the South Atlantic Anomaly. All data are sampled to a time resolution of 100 ms.

similar way. In case there exists no complementary information (eg. images obtained at other wavelengths as well as synthetic maps compiled from microwave interferometric observations) about the number and approximate positions of the sources, only the position of the integrated emission center within the field of view can be obtained by averaging φ_1' and φ_2'. It is in general not possible to decide whether the two different positions φ_1' and φ_2' result from two separated sources or from one extended source. However if complementary data exclude that the emission is due to one extended source, and also indicate the approximate positions of the sources, it is no more necessary to average the calculated positions φ_1' and φ_2'. They can now be taken as a reasonable guess for the positions of the two sources S_1 and S_2. It is important to notice that in the two dimensional case the complementary information may not only be due to independent observations but can also result from the interrelations of the flux levels observed by a two dimensional focal array in case the number of beams is > 3 (Sect. 4.1). This is in contrast to the one dimensional example discussed above where a separation of sources is only possible if their distance is larger than the HPBW.

Instead of switching off beams, a Gaussian weight can be used to average the positions. If this Gaussian is centered at e.g. φ_1' and its half power size is smaller than the distance between φ_1' and φ_2' the influence of the solution φ_2' in the averaged result will be strongly suppressed and hence the averaged position will be close to φ_1'. As our algorithm centers the Gaussian always at the latest calculated and averaged position, a considerable enhancement of the emission from the weaker source e.g. S_2, can lead to a change of the position of the emission center from one source to another, and therefore point out which of the sources is dominant (Sect. 4.1).

Hence switching off beams allows to find the positions of individual sources that emit at the same time, provided that the approximate source positions can be inferred from complementary information. On the other hand the Gaussian weighting can

be used to evaluate which of the sources is dominating the emission. In case of the event of May 9 the results obtained by both procedures have been cross checked. The relative displacement between the source positions that have been obtained by the two methods is less than 10" while their angular separation is about 75".

Finally it has to be mentioned that a change of brightness in the weaker source may distort the emission center position calculated near the dominant source. Hence in case of two sources emitting at the same time a careful discussion is necessary to decide whether positional structures observed within one source may be due to brightness changes in the other source or represent an original feature of the source under consideration (Sect. 4.2).

3. Microwave and hard X-ray observations

The event of May 9, 1991 occurred in NOAA region 6615 from 12:07:30 UT until 12:10 UT and was classified as a C6 flare in X-rays and as a 1N flare in the optical range. It produced a considerable microwave flux in two subsequent peaks with a flux maximum of about 400 sfu at 19.6 GHz. It was observed from 8.4 to 35 GHz and at 48 GHz at Bern and Itapetinga respectively. There are no data available at 3 and 5 GHz while the flux at 50 GHz is within the noise level of the Bern observations at this frequency. Due to the CGRO passing through the South Atlantic Anomaly before 12:08:15 UT, BATSE provided simultaneous observations only for the second of the two major microwave peaks.

3.1. Microwave total flux observations

Microwave and mm-wave time profiles at different frequencies are not always well correlated. The same is also true for hard X-ray time profiles in different energy ranges and their correlation with microwaves (see, for example, Kaufmann et al. 1983; Costa et al. 1984; Kundu et al. 1992; 1994). For the event studied here two impulsive peaks (hereafter peak 1 and peak 2) were observed with a duration of about 30 s each (Fig. 2, upper part). Both peaks differ considerably in spectral and pola rization properties. While the intensity profiles at 8.4, 11.8, 19.6 and 35 GHz result from the Bern total Sun observations without spatial resolution, the 48 GHz time profile results from the summation over all 5 channels of the multibeam telescope at Itapetinga.

The hard X-ray observations by BATSE during the second microwave peak exhibit a considerable level of fluctuations that are superimposed on the slower component. While the fluctuations cannot be detected in the microwave observations, the slow component of the hard X-ray time profile closely follows the evolution of the microwave intensity (Fig. 2, lower part).

The microwave spectra inferred from the discrete frequency observations are presented in Fig. 3. The turnover frequency (the frequency of the spectral maximum, hereafter f_{turn}) has been calculated with spline interpolation (full line) from the observed microwave spectrum at discrete frequencies (diamonds). The

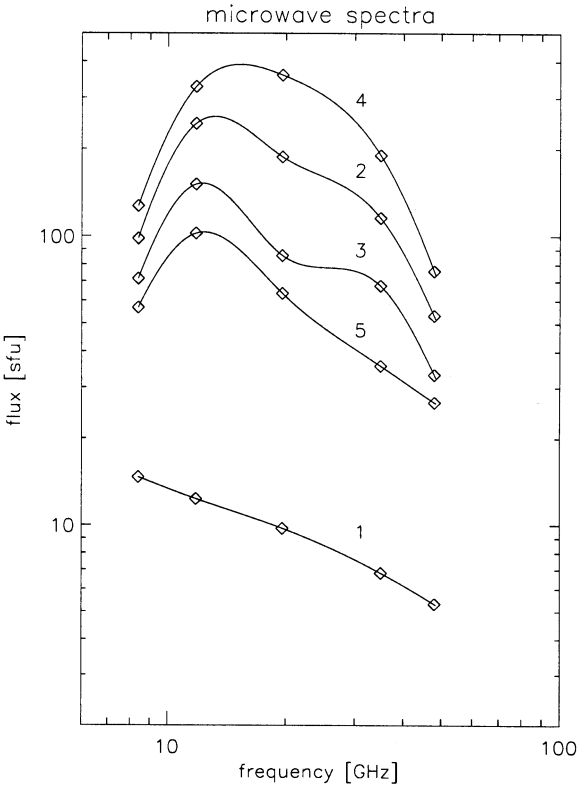

Fig. 3. Microwave spectra obtained from spline interpolation (full line) on the observed fluxes at discrete frequencies (diamonds). Spectrum 1 refers to the very beginning of the burst, spectrum 2 to the first flux maximum (peak 1), spectrum 3 to the onset of the second maximum and spectrum 4 to the second maximum itself (peak 2). Finally spectrum 5 shows the post burst situation.

labels refer to the times marked with small arrows in the time profile of Fig. 4. The preburst spectrum (1) evolves to a double hump spectrum at the maximum emission of peak 1 (2), with the turnover frequency around 13 GHz and a second hump at about 30 GHz. During the decay phase of peak 1 the second hump becomes more pronounced (3) while during peak 2 (4) the spectrum is very round and broad and the turnover frequency increases to about 16 GHz. In the decay phase only the low frequency component remains (5).

Spectral and polarization properties are presented in Fig. 4. The lowest plot shows the flux at 11.8 GHz while the evolution of the turnover frequency of the microwave spectrum is plotted above. There exists a considerable shift in f_{turn} from about 13 GHz during peak 1 to about 16 GHz during peak 2. It is important to note that the start of this shift is later than the flux minimum between the two peaks (vertical line in Fig. 4). The uppermost time profile shows the degree of circular polarization at 11.8 GHz. Again there exists a considerable difference between peak 1 and 2: while toward the decay phase of peak 1 the polarization increases to a relatively high level of 35% it sharply decreases to about 12% as soon as the emission of peak 2 becomes dominant. Finally during the decay phase this decrease vanishes and again the 35% level is established. The

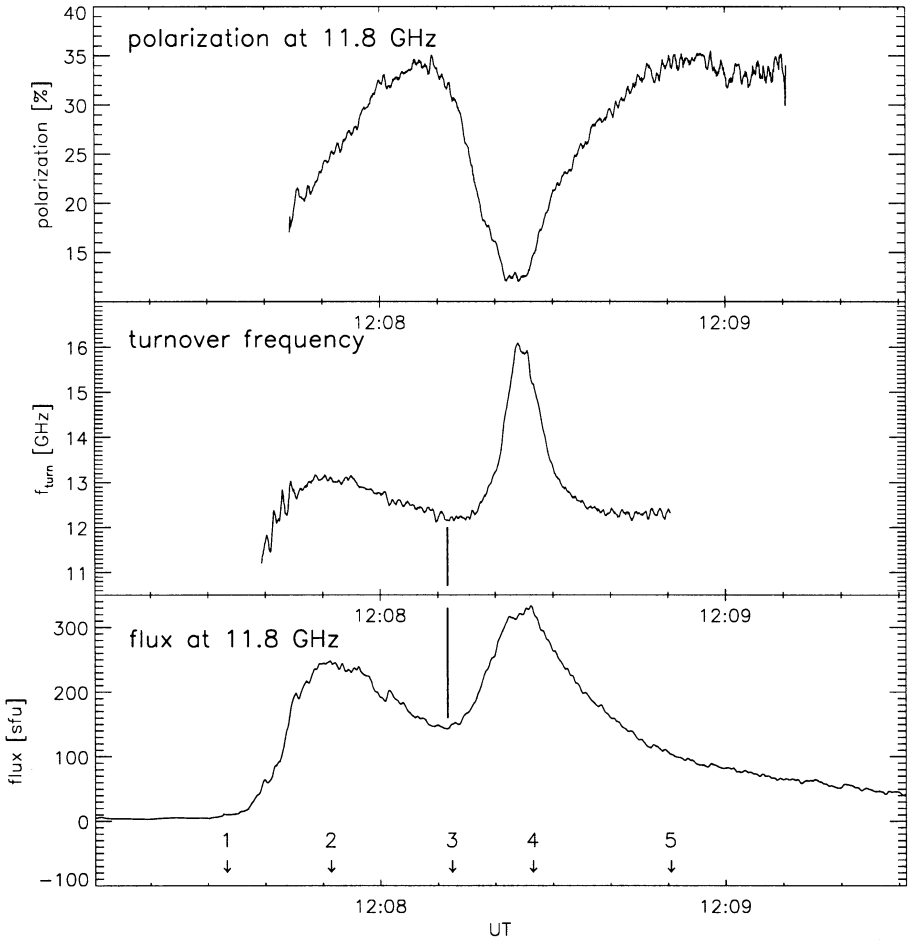

Fig. 4. Polarization and flux time profiles at 11.8 GHz as well as the evolution of the turnover frequency of the microwave spectra which has been inferred from a spline interpolation using the flux observations at 8.4, 11.8, 19.6, 35.0 and 48.0 GHz. The arrows with numbers indicate the times of the microwave spectra which are presented in Fig. 3.

same behavior, but less prominent, is visible at 8.4 and 19.6 GHz while at 35 GHz peak 2 results in a slight enhancement of the polarization of $\simeq$ 5%. The calculation of f_{turn} as well as the degree of polarization requires enhanced flux levels and hence are restricted to the time interval between 12:07:40 UT and 12:08:50 UT. The accuracy of absolute polarization measurements is $\cong$ 10% while for this specific event the detection of relative changes is limited by the noise level to about 1%.

3.2. Hard X-ray observations

Spectral and timing features of the hard X-ray observations are presented in Figs. 2 and 5. The photon count profiles on the upper left of Fig. 5 (from top to bottom the 25-55 keV, the 55-110 keV, the 110-300 keV and the $\geq$300 keV channel) show a considerable difference in time evolution: while the upper two time profiles look very similar the lower two are considerably delayed.

The photon spectra at the times labeled with A, B and C as well as the spectra of the fluctuations are plotted on the right. The center energies of the hard X-ray channels have been estimated by weighting the bandwidth with a power law of a spectral index of -2 while the error bars in energy result from a variation of the spectral index from 0 to -4. The errors of the photon fluxes are estimated from signal to noise ratios. The noise level of the order of 3×10^3 counts has been obtained from the noise of the post burst photon count profiles.

The delay of the 110-300 keV channel in relation to the 55-110 keV energy band results from a hardening of the spectrum above 80 keV after the maximum of peak 2 (spectrum C). This break in the photon count spectrum is not clearly visible in the spectra A and B which relate to the rising phase and maximum emission of peak 2. This is confirmed by the even further delayed maximum in the channel observing energies above 300 keV. Due to the low signal to noise ratio this channel could not be used to infer the spectrum. Timing features between different energy bands as well as between hard X-rays and microwaves will be discussed below.

A running mean (dotted lines in the upper left part of Fig. 5) has been subtracted from the original hard X-ray time profiles in order to enlarge the fluctuations, which are plotted in a normalized scale on the lower left of Fig. 5. They are about one order of magnitude above the noise level in the two lowest hard X-ray channels. A χ-square test performed on the original 64 ms data yielded a mean delay of the fluctuations at the 25-55 keV band in relation to the 55-110 keV band of 1 integration period (64 ms) for 80% of the fluctuations. Due to the low signal to noise ratio the fluctuations are not clearly visible in the 110-300 keV channel. However the maximum of the difference signal in this energy band allows to estimate the upper flux limit of the fluc-

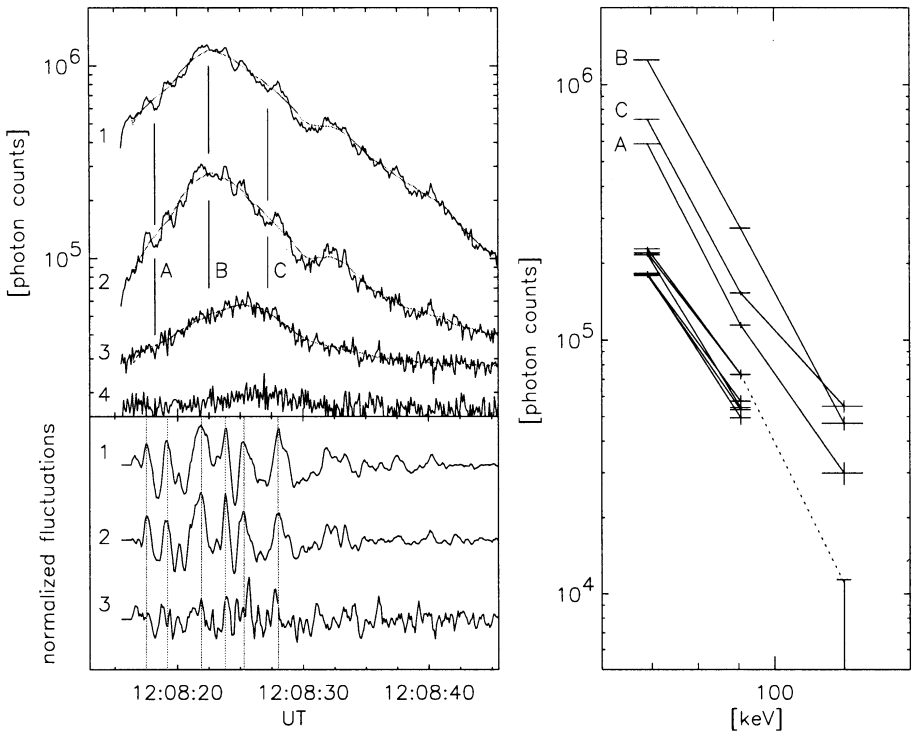

Fig. 5. Photon count spectra and fine structures of the hard X-ray observations. On the upper left the photon fluxes recorded in the energy bands of 25-55 keV, 55-110 keV, 110-300 keV and ≥300 keV are plotted (top to bottom). The full line represents the original data while the dotted line results from a running mean of 30 data points. Below the fine structures of the count time profiles are extracted and normalized in order to emphasize the similarities. On the right photon count spectra of the total count rate as well as the fine structures are plotted. Labels A,B and C refer to the total count spectra obtained at the times indicated on the left part of the figure. The group of spectra below shows the hard X-ray spectra of the fine structures which are always taken at the local count maximum. Error bars of the count rates are estimated from signal to noise ratios. A power law with an index of -2 has been used to obtain the mean energy of the hard X-ray channels. The error in energy is estimated assuming a maximal variation of the spectral index of ± 2.

Table 1. Relative timing of the microwave and hard X-ray emission during the rising phases of the microwave peaks 1 and 2. Delay times are in seconds and positive values indicate a delay relative to the 8.4 GHz microwave emission. Absence of data is represented by a horizontal bar. The uncertainty is approximately ± 0.2 s.

	peak 1	peak 2
[GHz]	delay of 80% flux [s]	delay of 80% flux [s]
8.4	0	
11.8	1.2	1.1
19.6	2.7	2.3
35.0	5.6	3.4
48.0	7.4	4.5
[keV]		
25-55	–	1.0
55-110	–	1.0
110-300	–	3.1
≥300	–	4.7

tuations (vertical bar on the lower right of Fig. 5). Hence the dotted line indicates the approximate spectrum of the fluctuations which is, above 80 keV, considerably softer than the total count spectrum after the maximum of peak 2 (spectrum C).

3.3. Timing of microwave and hard X-ray emission

The relative timing properties of the emission at different microwave frequencies as well as at different photon energies are summarized in Table 1.

The relative timing during the rising phases has been evaluated at 80% of the maximum peak emission. The 80% flux relates to the preburst level for peak 1 and to the minimum between the two peaks for peak 2. All values refer to the 8.4 GHz microwave flux and a positive sign indicates a delay with respect to this frequency. In general the radio emission at higher frequencies as well as the hard X-ray emission at higher energies are increasingly delayed towards the 8.4 GHz emission. Delays reach maximum values for the 48 GHz emission of 7.4 s for peak 1 and 4.5 s for peak 2 with respect to the 8.4 GHz emission. The hard X-ray emission is delayed by 1 to 4.7 s for the 25-55 keV and the ≥300 keV channel respectively. It has to be noted that the 55-110, 110-300 and the ≥300 keV emission are increasingly delayed while there exists no time lag between the emission in the two lowest energy bands (25-55 keV and 55-110 keV). For comparison, the time shifts of the maximum of the cross correlation function between different channels have been calculated. The results for the rising phases of peak 1 and peak 2 confirm the delays obtained at the 80% levels.

The fluctuations on the hard X-ray time profile for the second burst structure do not seem to have counterparts in the microwave time profiles. However, this comparative analysis is further complicated by the low sensitivity (≈ 10 sfu) of the Bern data and also due to a qualitative trend which indicates that the relative amplitude of fluctuations reduces with frequencies to about 5% of the total flux below ≈ 30 GHz (Correia et Kaufmann 1987).

4. Spatially resolved observations

The multibeam technique used at the Itapetinga Radio Observatory allows to find the most probable position of the mm-wave

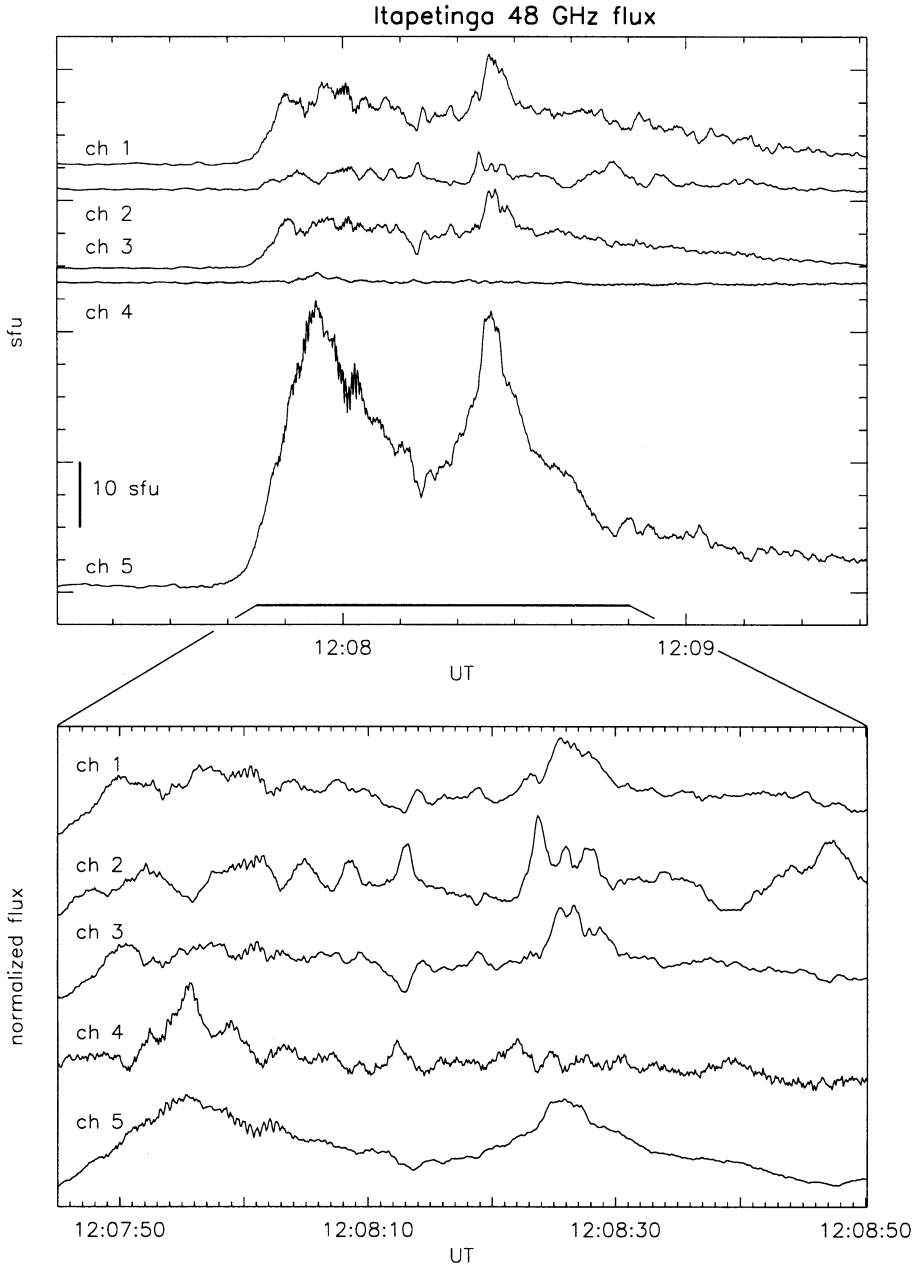

Fig. 6. Total power time profiles observed with the 5 channels of the multi beam radiometer at Itapetinga. The upper half of the figure shows the calibrated fluxes during the whole event while below the time interval with the most intense variations has been expanded and normalized in order to emphasize the differences in the time profiles.

emission center within the field of view of $\approx 6' \times 4'$ (Herrmann et al. 1992). However in this case with two sources that emit at the same time (Sect. 4.1) the general features of the flux relations between 4 different channels (where each channel corresponds to a separate beam observing a slightly different region on the Sun) are discussed first in order to get a qualitative overview before the numerical results are presented.

4.1. Overall source geometry

The single channel flux measurements are presented in Fig. 6. Calibrated flux time profiles of the whole event are plotted on the upper half. Channels 1 and 3 exhibit roughly the same flux levels, while channel 2 reaches only about half of these values. The observed flux in channel 4 is very small while channel 5 clearly dominates. The time interval for which emission center positions have been calculated (12:07:45 UT until 12:08:50 UT) is expanded below in order to emphasize the changes. The fluxes in all channels have been normalized. For some of the structures phase relations between single channels (e.g. at 12:08:13 UT) do exist but they are not the same throughout the event. This clearly excludes the possibility that the fluctuations are due to an antenna movement or oscillation which requires systematic phase relations between different channels. Furthermore such strong levels of fluctuations would require antenna movements larger than 10" at least which can be excluded from the simultaneously recorded outputs of the antenna position encoders.

Fig. 7 sketches the beam geometry used during the observing campaign in May 1991. The circles represent the HPBW of

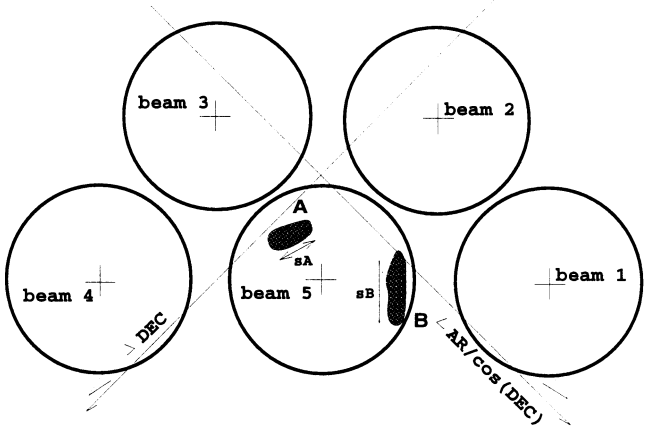

Fig. 7. Sketch of the beam geometry at the antenna focus during the observation period of May 1991 in offsets of equatorial coordinates relative to the antenna pointing. The factor 1/cos(DEC) is included in order to avoid image distortion due to spherical coordinates. The circles indicate the beams at half power sensitivity (diameter 2') while the two hatched regions represent the approximate positions of the two microwave sources. The arrows sA and sB indicate the two possibilities of subsource alignment discussed in Sect. 4.2.

the 5 beams while the dark, hatched regions mark the approximate positions of the two main microwave sources as inferred from numerical calculations. As mentioned above the flux levels detected with the beams 1 and 3 are about the same. Hence in case of one single source its position should be at approximately the same distance from beam 1 and beam 3. On the other hand, the flux level corresponding to beam 2 is only about half of the ones detected with beams 1 and 3. The only possible solution for one single source lies on the extension of the straight line connecting the centers of the beams 2 and 5 but beyond beam 5. This in turn requires that beam 2 should observe much less flux in relation to beam 5 than it actually does. Hence there does not exist a position for a single source that consistently explains the observations with all beams and one has to resort to a multi source interpretation (Sect. 2.2).

The dynamic burst map in Fig. 8 presents the 2-d distribution of the emission centroid position during the time of considerably enhanced emission from 12:07:45 UT till 12:08:50 UT. It results from the positional distribution of 17000 emission centroid determinations, each one obtained from 4 ms of observations. Contour levels are linearly scaled, the maximum amounts to 423 positional counts within a square of 2" $\times$ 2". Coordinates are increments in declination ($\triangle\delta$) and right ascension ($\triangle\alpha$) relative to the pointing of the antenna axis. The factor $1/cos(\delta)$ is included to avoid image distortion due to spherical coordinates.

Depending on the initial starting position one of the two sources labeled with A and B in Fig. 8 is obtained by the calculations (Sect. 2.2). Starting the calculation at a position near source A, the emission center remains at A from 12:07:45 UT until 12:08:12.5 UT and then moves to the position of source B. Hence it can be concluded that before 12:08:12.5 UT (peak 1) source A is dominant, while later on (peak 2) source B dominates. Which source is dominant during the decay phase cannot be definitely concluded because in this phase the emission center largely scatters around source B but does not move back to source A. However it has to be emphasized that both sources should emit during the whole event due to the qualitative arguments discussed above. The spatial separation of the two sources is approximately 75" which equals $5.4 \cdot 10^9$ cm. Even if this value represents a lower limit only (Sect. 2.2) the low flux observed with beam 4 is not consistent with a position of source A that is considerably shifted further apart from source B (Figs. 6 and 7).

4.2. Subsources

As mentioned above the fluctuations with a time scale of a few seconds that can be seen most prominently during peak 1 in the channels 1 to 3 (Fig. 6, lower part) cannot result from antenna movements (Sect. 4.1). Furthermore the complex phase relations, due to correlated or anticorrelated flux variations between different channels which change in time do not allow to attribute the fluctuations to a single, pulsating source (Fig. 6). Hence the fluctuations are expected to be due to movements of the emission center on the Sun. This can either be due to the movement of a physical source or the brightening of several spatially separated sources at different times. The two-source configuration as inferred above therefore allows two possible situations that need to be investigated: i) the fluctuations result from internal positional changes of the emission center within source B or ii) they result from internal movements within source A.

A close inspection of the phase relation between channel 2 and 3 in the time interval from 12:07:55 UT until 12:08:15 UT revealed an off phase relation that can only result if the emission center quasi periodically changes between two positions of which one is closer to beam 3 and the other one closer to beam 2. As the fluctuations are hardly visible in channel 5 the change in position must be about tangential to beam 5. A movement of the emission center within source B is therefore restricted to an approximately vertical direction (arrow sB in Fig. 7) and hence the fluctuations in the beams 2 and 3 must be in-phase, in contradiction to the observations. On the other hand a movement within source A (arrow sA in Fig. 7) can as well be tangential to beam 5 as also accommodates the phase relation between channel 2 and 3. Hence we conclude that the strongly fluctuating signals during peak 1 must be due to positional changes of the emission center within source A.

Fig. 9 presents the results of the position calculations for 4 strong fluctuations during peak 1 (source A in Fig. 8). The time profile on the upper part of Fig. 8 shows the difference between the flux originally detected in channel 2 and a strongly smoothed time profile. Regions where the difference flux is larger than $\pm$ 0.5 sfu are marked with black color. Reduced flux levels are labeled with D1 to D4 while enhanced fluxes are labeled with U1 to U4. The dynamic burst maps below consist only of emission center positions that have been calculated during the times of large deviations from the mean flux level (time intervals marked

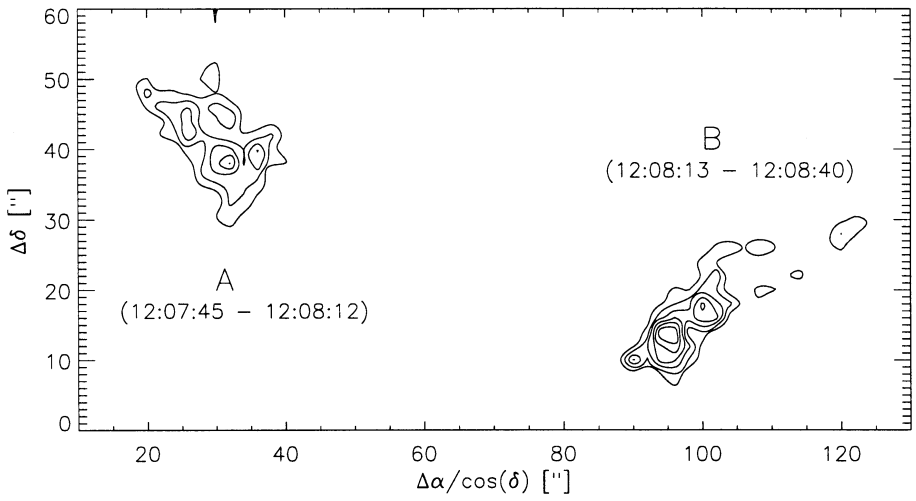

Fig. 8. Dynamic burst map of the emission center distribution during the whole event. The grid spacing is 2" and approx. 17000 positions each one calculated within 4 ms during the time interval from 12:07:45 UT until 12:08:50 UT have been used. Before 12:08:12.5 UT emission from source A dominates while for later times source B is dominant. Coordinates refer to offsets in right ascension and declination relative to the antenna pointing.

with black color on the difference time profile). There exists a clear separation of the sources that belong to the enhanced and the ones that belong to the reduced flux levels. The center of source A (Fig. 8) lies approximately in the middle between the U and the D sources. The separation between the subsources is largest for the sources D1 and U1 with approx. 21" while it reduces to about 12" between the sources D4 and U4. Besides the obvious bouncing of the emission center between the U and D positions with a time scale of 2 to 4 s a drift from the upper right to the lower left is superimposed. The distance between the sources U1 and U4 is about 20" while between D1 and D4 it is about 13". Finally it has to be emphasized that a detailed analysis of the positional scatter of the emission center of the subsources showed that especially source D4 is very stable in position from 12:08:09.3 UT till 12:08:11.3 UT within 2" × 2".

The intense local maximum at 12:08:13 UT in channel 2 following the time interval D4 is not included in the above analysis, as its behavior is essentially different. The signals in the channels 1 and 3 exhibit much stronger changes in flux than during the fluctuations before, and this leads to the movement of the emission center from source A to source B at 12:08:12.5 UT.

A similar analysis as the one described above has been used in order to determine positions of substructures of source B during peak 2. However there exist no such simple phase relations as for the subsources of source A and hence there is no strong evidence that allows to attribute the fluctuations during peak 2 to one of the two sources (A or B). Therefore we have to speculate that even if the emission of source B dominates for times after 12:08:12.5 UT the fluctuations visible in the time profiles of the channels 1, 2 and 3 are most probably due to a superposition of positional changes within source B as well as within source A during peak 2. In any case, the time profiles definitely exclude the possibility that the fluctuations are due to an alternate brightening of the sources A and B, as especially channel 1 would show much stronger fluctuations in this case. This is a first evidence that small scale space structures are present throughout the whole event.

Finally it has to be mentioned that, apart from the fluctuations discussed above, a much faster ripple superimposed on all 48 GHz time profiles appears between 12:07:58 UT and 12:08:04 UT, with a time scale of a about 500 ms. The investigation whether or not this ripple is due to solar emission is still in progress and will be published later.

5. Discussion

The general features of the microwave and hard X-ray observations will be discussed now, in order to demonstrate that the 'trap plus precipitation' hypothesis allows a consistent interpretation of the observations. At the end possible explanations for the small scale structures within source A will be outlined.

5.1. Microwave emission from two sources with opposite magnetic polarity

As discussed in Sect. 3.1 the polarization and spectral properties differ drastically for the two major time structures. The high degree of polarization during and especially in the decay phase of peak 1 suggests that emission from a region of one magnetic polarity dominates. The further increase of polarization after the flux maximum of peak 1 might be due to a decrease of optical thickness. The additional flux of peak 2 is about 150 sfu at 11.8 GHz which is approximately equal to the flux level which remained from peak 1 at the beginning of peak 2. If the source responsible for peak 2 were unpolarized then the degree of polarization should be reduced from 35% to about 17%. As the polarization is reduced to about 12% the source responsible for peak 2 most probably emits radiation of opposite polarization. However the reduction of polarization is known from other examples and might be also explained by an increase of the optical depth.

The increase of the polarization after the impulsive phase of peak 2, to the value observed during peak 1, leads to the suggestion that the source responsible for peak 1 still emits, while the emission from the second source decays more rapidly. Hence the reduction of polarization during peak 2 is unlikely due

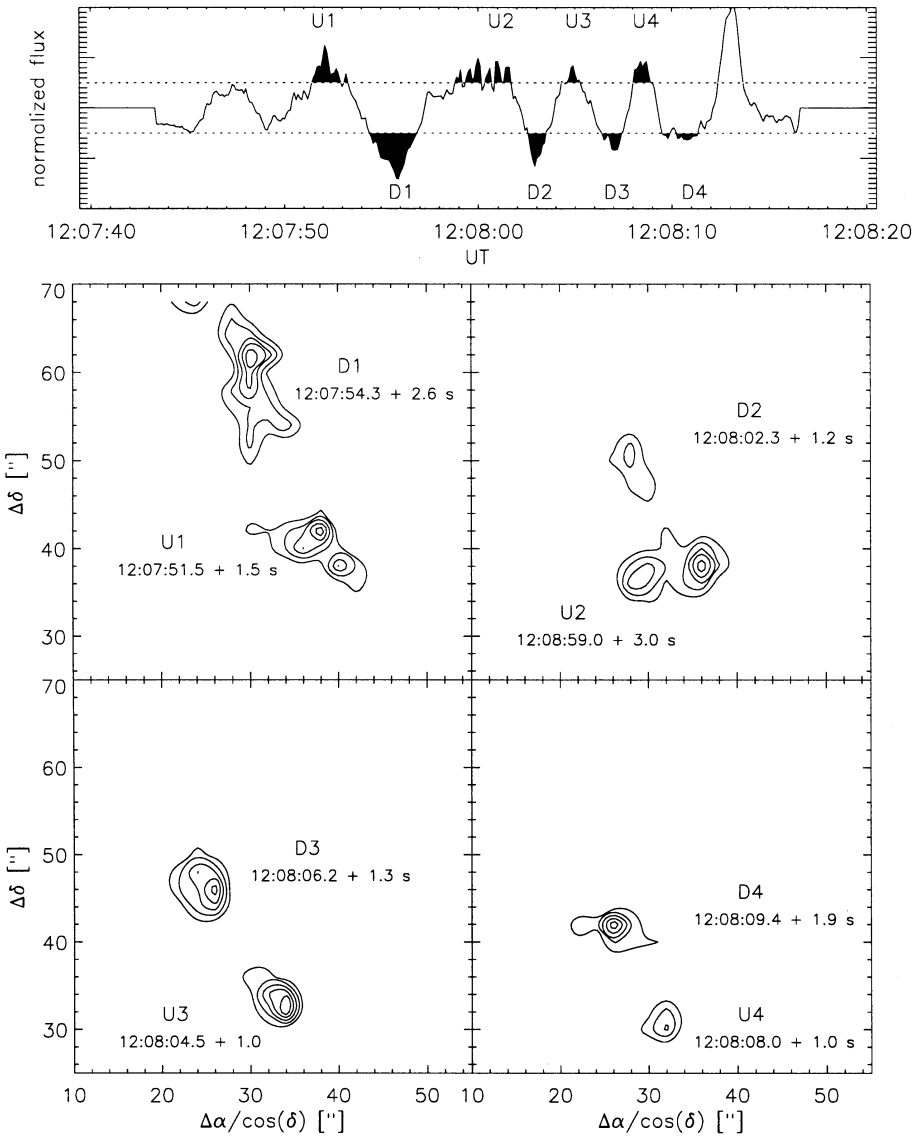

Fig. 9. Positions of subsources of source A. The upper plot shows the expanded flux profile of channel 2. A running mean has been subtracted and 8 time intervals with a flux difference of more (U1 to U4) or less (D1 to D4) than 0.5 sfu are emphasized. The dominating positions of the emission during these intervals are shown on the contour plots below. For this dynamic maps only the emission center positions of the emphasized time intervals U1 to U4 and D1 to D4 are used in order to demonstrate the positional separation between the U and D regions. The resolution of the dynamic burst maps is 1".

to a rapid decay of the emission of peak 1 and the superposition of emission from an unpolarized source. This description favors the suggestion that the microwave emission of peak 1 and 2 originates from two different sources which may be lying within regions of different magnetic polarity.

This scenario is further supported by the analysis of the microwave spectra presented in Fig. 3. The spectra observed at the maximum emission of peak 1 and 2 are definitely different. While during peak 1 f_{turn} is around 13 GHz, it is most likely that the contribution of the second spectral hump around 30 GHz becomes dominant during peak 2. This may explain the shift of f_{turn} to about 16 GHz as well as to the broad spectrum during peak 2. Both features vanish during the final decay phase. This is in good agreement with the discussion of the polarization properties and confirms that peak 2 is most probably due to a source with different source parameters. The shapes of the microwave spectra also exclude that the emission is due to one, homogeneous source. The double hump spectrum visible during peak 1 clearly needs an inhomogeneous source to produce the two spectral components, while the broad and round spectrum during peak 2 very unlikely results from a homogeneous source. A systematic variation of the source parameters in a homogeneous model has been used to calculate more than 2000 microwave spectra but no such broad spectra could be obtained (F. Merz 1994, private communication). For specific events the same conclusions have been obtained by several authors (e.g. Zodi 1991; Herrmann et. al. 1994).

It has been demonstrated in Sect. 4.1, that the 48 GHz emission is due to two different sources, spatially separated by about $5.4 \cdot 10^9$ cm and that both sources emit during the whole event. Furthermore one source dominates the emission during peak 1 while the other dominates during the second peak. This agrees with the conclusions inferred from polarization and spectral observations. The suggested presence of subsources centroids of emission agrees with mm-waves BIMA results for certain bursts, for which the emission is dominated by sources with

diameters of a few arcseconds (Lim et al. 1992). Hence we suggest that the observed emission originates from a loop connecting the two 48 GHz sources which are expected to result from the highest field strengths and hence from lowest altitudes (Dulk et al. 1985). During peak 1 the emission preferentially originates from one leg of the loop while for peak 2 emission from the other leg dominates.

5.2. 'Trapping plus precipitation' inferred from hard X-ray observations

The hard X-ray observations obtained by BATSE reveal two different features: a spectral hardening throughout the event and superimposed fluctuations that show in 80% of the cases a delay of the lower energies of $\simeq$ 64 ms.

5.2.1. Total count observations

The spectral hardening agrees with the predictions made by the 'trap plus precipitation model', where scattering of the trapped electrons into the loss cone is energy dependent and more likely for the less energetic electrons. A detailed discussion of the energy dependence of the electron scattering requires that the 3 different regimes of weak, moderate and strong diffusion are considered separately. While in the weak diffusion limit the hardening of the electron spectrum results from the dominant coulomb scattering (e.g. Vlahos et al. 1984 for a review), it has been shown that due to wave particle interactions a similar energy dependence exists also in the strong diffusion limit (Bespalov et al. 1987, hereafter referred to as BZS). For the intermediate regime of moderate diffusion on the other hand a nearly constant shape of the electron spectrum is expected (e.g. Trottet et Vilmer 1984).

Numerical computations of the energy dependent time delay (due to the spectral hardening) for the 'trap plus precipitation' model in the weak diffusion limit (Trottet et Vilmer 1984) predict a continuous increase of the delay with energy, depending on the density of the trap. On the other hand only a very weak dependence of the delay on energy is expected in case of moderate diffusion. However it is very likely that at energies $>$ 100 keV resonant scattering of particles becomes important (Melrose et Brown 1976; Wentzel 1976; BZS) and hence the assumption of dominant coulomb scattering is no longer satisfied. Therefore the density of the trap cannot be inferred from the delay time due to the high energy above which the delays are detected ($>$ 100 keV). On the other hand the absence of a delay between the 25-55 keV and the 55-110 keV channel could be an evidence for moderate diffusion in this energy range. Hence we suggest that the delays observed above 100 keV are due to strong, turbulent diffusion as suggested by BZS while the absence of delays between the 25-55 keV and the 55-110 keV channel results from electron scattering in the regime of moderate diffusion. The energy E_{min}= 100 keV of the transition from moderate to strong diffusion allows to estimate the Alfvén velocity within the loop (Melrose et Brown 1976; BZS):

$$E_{\min}[keV] \approx 5.2(\frac{v_A[cms^{-1}]}{10^8})^2.$$

For E_{min}= 100 keV an Alfvén velocity of $v_A = 4.4 \times 10^8\, cm\, s^{-1}$ results. The mirror ratio of the trap $\sigma = B_{foot}/B_{top}$, where B_{foot} and B_{top} are the magnetic field strength at the mirror point and the top of the trap respectively, can be estimated from the corresponding Alfvén velocity (BZS):

$$t_{ls}^e \approx \frac{m_e}{m_i}\left(\frac{v}{v_A}\right)^2 \sigma t_c.$$

v is the speed of the 100 keV electrons, $t_c = l/2v$ the travel time of free streaming electrons moving from the top of the loop to the footpoints and t_{ls}^e the approximate travel time of the electrons in the strong diffusion limit. The observed delay of $\approx$ 2 s between the 55-110 keV and the 110-300 keV channel allows to evaluate the mirror ratio as σ = 10 in the case of 100 keV electrons (the approximate energy of the transition from moderate to strong diffusion). The Alfvén speed as well as the mirror ratio are within the range required for particle scattering in the strong diffusion limit (BZS) while the loop length of l =8.4$\times$10^9 cm, that has been estimated from observations, is at the uppermost limit of the values required for strong diffusion (BZS). However it has to be mentioned that BZS also derive a minimum level of particle source power required to generate a sufficient level of whistler turbulence for strong diffusion. With the available observations we cannot prove that enough energetic particles per unit volume and time have been accelerated during the impulsive phase to overcome this threshold level.

5.2.2. Fluctuations

The time lag of the fluctuations in the 25-55 keV channels towards the ones at the 55-110 keV channels suggests that the fluctuations are due to the primary energy release mechanism and hence the time difference is a time of flight effect. Using the geometry discussed above and assuming that the electrons have to travel approximately half of the semicircular loop the distance from the release region is 4.2$\cdot$10^9 cm. The mean energies inferred for the 25-55 keV and the 55-110 keV band are 35 keV and 75 keV respectively. This results in an expected time lag of the 35 keV electrons towards the 75 keV electrons of about 100 ms. This agrees as an order of magnitude estimate with the 64 ms deduced from observations (Sect. 3.2).

We therefore suggest that the spectral hardening results from a 'trap plus precipitation' situation in a loop connecting the two 48 GHz sources, while the fluctuations in the hard X-ray time profile are due to electrons with energies $\leq$ 100 keV and low pitch angles. Due to their energies below E_{min} these electrons should not be affected by the scattering in the strong diffusion regime and therefore directly precipitate to dense regions at low altitudes where they emit thick target emission. Furthermore the low pitch angle of these electrons is expected to inhibit efficient emission of microwaves. This implies that the fluctuations are not due to a modulation of the energy transport from coronal

to chromospheric levels but represent features of the primary energy release.

It has to be mentioned that even if the predictions of the 'trap plus precipitation' model agree with the observations we cannot exclude that the whole observed features are dominated by the primary energy release. In this case the electron acceleration mechanism not only needs to produce the fluctuations but also the spectral hardening, accelerating electrons to preferentially higher energies in the decay phase of the burst.

5.3. Small scale structures

The observations of subsources presented in Sect. 4.2 are the first proof of highly structured and inhomogeneous sources at 48 GHz. This is consistent with spatially resolved microwave observations at cm and mm wavelengths (e.g.: Alissandrakis 1986; Kundu et al. 1990, for reviews) and with imaging hard X-ray observations which also revealed multiple sources with a separation of a few arc seconds (e.g.: Sakao et al. 1992).

The subsources of source A may be due to i) an exciter or emitter that quasi periodically moves from the U to the D sources (Fig. 9) and hence it has to be suspected that the U and D sources are connected by small scale loops and that the neutral line separates the regions of the U and D sources or ii) the whole source A represents the foot point region of several closely related loops connecting the sources A and B. In this case the bouncing of the emission center would be due to several injections of electrons into primarily two close and parallel loops that connect regions of opposite magnetic polarity. Which case applies cannot be inferred from available observations and we have to restrict ourselves to the statement that we do see small discrete structures within source A, that there exists a quasi periodic change of the emission center position and that the emission center of subsources stays within 2" $\times$ 2" as long as 2 s.

6. Conclusions

Observations of the dynamic evolution of the 48 GHz emission center position, together with microwave- and hard X-ray spectra, allowed us to get a consistent picture of the overall features of this flare. We demonstrated that the emission is most probably dominated by non-thermal electrons partly trapped in a loop which connects the two 48 GHz sources and we suggest that the observed delays are due to scattering of precipitating electrons on the turbulence they generate (following the analysis by Bespalov et al. 1987). For the first time we could separate two simultaneous existing sources with a separation of little more than the half HPBW using a multibeam telescope. Furthermore, observations of small scale structures in one of the mm-wave sources were presented, including substructures with emission centers which stay within 2" $\times$ 2" as long as 2 s. Unfortunately the lack of simultaneous high spatial resolution observations in hard X-rays or H_α- images or magnetograms does not allow to investigate further the related physical processes. Finally it has to be emphasized that even a flare that exhibits only two major time structures in the spatially unresolved observations presents a very high degree of inhomogeneities. Hence simultaneous spatially high resolved observations at different wavelengths are definitely necessary.

Acknowledgements. CRAAE is jointly operated by the Universities of São Paulo, Campinas and Mackenzie and by the National Space Institute, INPE. The project was supported by the Swiss National Science Foundation under grant No. 20-36417-92.

References

Alissandrakis C.E., 1986, Solar Phys. 104, 207
Bespalov P.A., Zaitsev V.V., Stepanov A.V., 1987, Solar Phys. 114, 127
Bruggmann G., Magun A., 1990, A&A 239, 347
Correia E., Kaufmann P., 1987, Solar Phys. 111, 143
Costa J.E.R, Kaufmann P., Takakura T., 1984, Solar Phys. 94, 369
Costa J.E.R, 1994, private communication
Dulk G.A., Bastian T.S., Kane S.R., 1985, ApJ 300, 438
Fishmann et 16 al., 1989, Proc. GRO Science Workshop, ed. W.N. Johnson, 2-39
Georges C.B., Schaal R., Costa J.E.R., Kaufmann P., Magun A., 1989, SBMO-International Microwave Symposium/Brazil IEEE Catalog, No 89th0260-0, vol. II, 447
Herrmann R., Magun A., Costa J.E.R., Correia E., Kaufmann P., 1992, Solar Phys. 142, 157
Herrmann R., Rolli E., Correia E., Costa J.E.R., 1994, Solar Phys. 149, 155
Kaufmann P., Strauss F.M., Costa J.E.R., Dennis B.R., Kiplinger A., Frost K.J., Orwig L.E., 1983, Solar Phys. 84, 311
Kundu M.R., White S.M, Gopalswamy N., Biejing J.H., Hurford G.J., 1990, ApJ 358, L69
Kundu M.R., White S.M., Gopalswamy N., 1991, MAX 91 Workshop 2, eds. R.M. Winglee and B.R. Dennis, p. 119
Kundu M.R., White S.M., Gopalswamy N., Lim J., 1992, Second GRO Science Workshop, NASA CP-3137
Kundu M.R., White S.M, Gopalswamy N., Lim J., 1994, ApJ. Suppl. 90, 599
Lim J., White S.M., Kundu M.R., Gary D., 1992, Solar Phys. 140, 343
MacKinnon A.L., Brown J.C., Trottet G., Vilmer N., 1983, A&A 119, 297
Melrose D.B., Brown J.C., 1976, Mon. Not. R. Astron. Soc. 175, 15
Merz F., 1994, private communication
Sakao T. et 11 al.: 1992, Publ. Astron. Soc. Japan 44, L83
Trottet G., Vilmer N., 1984, Adv. Space Res. 4, 153
Vilmer N., 1987, Solar Phys. 111, 207
Vlahos L., Machado M. E., Ramaty R. J., and 23 co-authors, 1984, in: Energetic Phenomena on the Sun NASA CP 2439, eds. M. Kundu and B. Woodgate
Wentzel D.J., 1976, ApJ 208, 295
White S.M., Kundu M.R., 1992, Solar Phys. 141, 347
Zodi Vaz A. M., 1991, Multiplas Popúlações de Particulas Aceleradas em Explosões Solares, Doctorate dissertation, INPE, Brasil

This article was processed by the author using Springer-Verlag LaTeX A&A style file *L-AA* version 3.